POLLUTION IN THE FREE TROPOSPHERE: GEOMETRICAL, OPTICAL, AND MICROPHYSICAL CHARACTERIZATION WITH MULTIWAVELENGTH RAMAN LIDARS

Ina Mattis[1], Detlef Müller[1], Albert Ansmann[1], Dietrich Althausen,[1] and Ulla Wandinger[1]

[1] *Leibniz Institute for Tropospheric Research, Permoser Str. 15, 04318 Leipzig, Germany, E-mail: ina@tropos.de*

ABSTRACT

We analyzed multiwavelength Raman lidar observations which were performed 1997-2004 at Leipzig, Germany, 1997 in Portugal, and 1999/2000 at the Maldives. Free-tropospheric aerosol layers were advected to the three measurement sites from different source regions. Trajectory analysis and tracer calculations were used to identify mineral dust from Africa and Arabia, forest-fire smoke from Siberia and North America, anthropogenic pollution from India, Southeast Asia, North America and Europe as well as aged anthropogenic aerosols from polar regions.

We characterized the aerosol types from the different source regions in terms of frequency of occurence, geometrical, optical and microphysical properties. The aerosol types (marine particles, mineral dust, forest-fire smoke, and anthropogenic particles) can be distinguished by their characteristic signatures in effective radius, single-scattering albedo (ssa), depolarization, and in the wavelength dependence of backscattering, lidar ratio, and extinction.

1. INTRODUCTION

Aerosols in the free troposphere have a comparably large lifetime and are often transported over long distances. Such inter-continental transport events may play an important role in the global aerosol cycle. Furthermore free-tropospheric aerosol particles can act as condensation nucleii and as such affect cloud and rain properties on a global scale.

Free-tropospheric aerosol layers are often optically thin. They are difficult to characterize with passive remote-sensing instruments because the layers are masked by the underlying planetary-boundary-layer (PBL) aerosols. Vertically resolved lidar measurements therefore are an indispensable tool to study PBL aerosol and free-tropospheric aerosol layers independently from each other.

2. INSTRUMENTS AND CAMPAIGNS

Our study is based on free-tropospheric aerosol layers observed over Leipzig since 1997 with the stationary IfT aerosol-temperature-humidity Raman lidar. Data were also collected during several field campaigns with the mobile IfT scanning 6-wavelength aerosol Raman lidar.

The stationary Raman lidar, which is kept in the upper floor of the institute's main building, is described in Ref. [1]. The system emits laser pulses at 355, 532, and 1064 nm with one Nd:YAG laser. The laser beam is expanded 15-fold and vertically transmitted into the atmosphere. The backscatter signals are collected by a 1-m Cassegrain telescope and transmitted to the signal detection unit.

The mobile Raman lidar, which is housed in a seatainer, is described in Ref. [2]. The system emits laser pulses at 355, 400, 532, 710, 800, and 1064 nm with the use of 4 lasers. A beam combination unit aligns all 6 laser beams onto one optical axis. The laser beam is expanded 10-fold and transmitted into the atmosphere with a turnable mirror. The backscatter signals are collected by a 0.5-m Cassegrain telescope and transmitted to the signal detection unit.

Polychromators are used for separating the signals at the different wavelengths. Interference filters in front of the detectors only transmit the backscatter signals at the desired wavelengths. Signals are detected with photomultipliers. The signals are collected on the basis of computer cards that operate with a sampling rate of 300 MHz. The detectors for the channels at 400, 710, and 800 nm of the 6-wavelength lidar are operated in the analog mode. 12-bit analog-digital converters are used to transfer these analog signals.

We developed an inversion algorithm to derive microphysical particle properties from the measured optical data. The software is based on inversion with regularization. It has been shown that only the combined use of the three (6) particle backscatter and two extinction coefficients provides trustworthy parameters of particle size, mean complex refractive index, and ssa [3]. A further improvement of the inversion algorithm towards a 2-dimensional regularization is presented in [4].

Both lidars deliver profiles of:
- backscatter coefficient at 3 (6) wavelengths,
- extinction coefficient at 355 and 532 nm,
- lidar ratio at 355 and 532 nm,

- depolarization ratio at 532 (710) nm,
- Ångström exponent,
- effective radius,
- surface-area and volume concentration,
- complex refractive index,
- single-scattering albedo.

Measurements with the stationary Raman lidar were performed in the framework of the European Aerosol Research Lidar NETwork [5] (EARLINET). We observed mineral dust from Africa, forest-fire smoke from Siberia and North America (NA) as well as anthropogenic pollution from NA and from polar regions in the free troposphere over Leipzig.

The outflow of anthropogenic pollution from Europe was characterized with the mobile Raman lidar during the Aerosol Characterization Experiment 2 (ACE 2) in Portugal [6]. During the Indian Ocean Experiment (INDOEX) mineral dust from Arabia and East Africa and anthropogenic pollution from India and Southeast Asia were observed with this lidar [7].

The different source regions and aerosol types were identified with trajectory analysis (HYSPLIT trajectories [8], FLEXTRA trajectories [9], and KNMI trajectories [10]) and FLEXPART tracer transport simulations [11].

3. FREQUENCY DISTRIBUTION

Regular measurements (EARLINET time schedule, 3 to 4 times per week) were performed in Leipzig from January 1997 to fall 2004. We retrieved 640 regular measurements at predefined dates within this 8-year time period. We derived frequency distributions of the occurence of aerosol layers from different source regions for this data set, but not for the field campaigns (maximum duration 1 year). In about 45% of the regular EARLINET measurements we observed free-tropospheric layers over Leipzig. Pollution from NA shows a maximum of occurence in summer, see Fig.1. Such layers were detected in 30% of all regular measurements in June. Aged anthropogenic pollution from north of 70° N has a maximum in spring and Saharan dust has two maxima, one in spring and one in fall. the overall frequency of Saharan dust events is low compared to pollution transport from NA.

4. GEOMETRICAL PROPERTIES

Fig. 2 shows the distribution of the bottom height, top height, and geometrical depth of the free-tropospheric layers. If a measurement case is characterized by several free-tropospheric layers (30% of the cases), the bottom height was calculated for the lowest layer, and the top height was calculated for the top most layer.
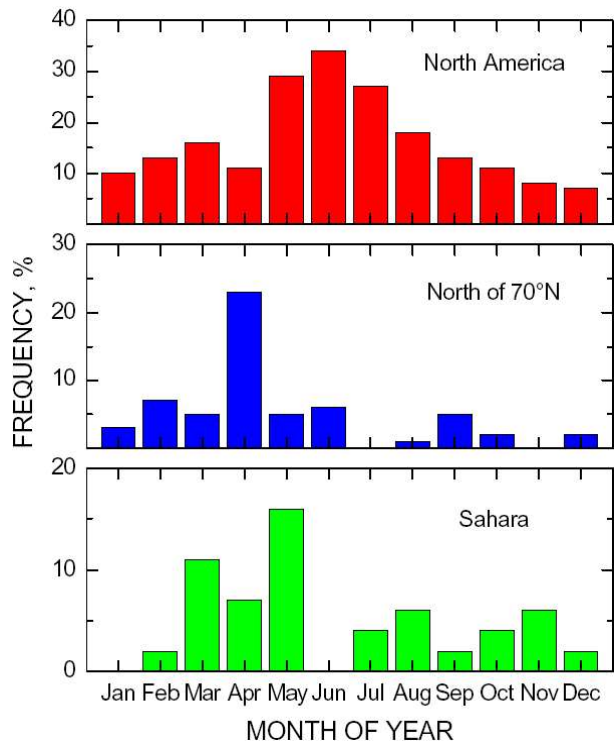
Fig.1. Frequency of free-tropospheric pollution transported from different source regions to Leipzig in the years 1997-2004.
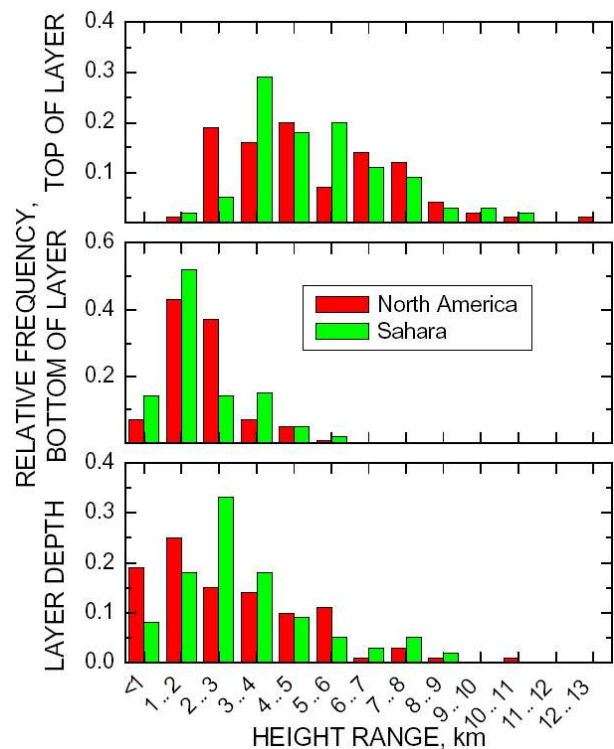
Fig.2. Frequency distribution of bottom and top height, and geometrical depth of free-tropospheric layers.

The bottom of the lower-most free-tropospheric layer is at or above 2-km height in approximately 45% of all cases. About 50% of the pollution layers were not geometrically separated from the planetary boundary layer. We used the trajectory information to estimate if those layers were residual layers of local origin or whether they were caused by long-range transport. We need more studies based on temperature and humidity profiles to strengthen the discrimination between local residual layers and long-range transport layers wich are not geometrically separated from the PBL. The top height of the free-tropospheric layers and their geometrical depth are higher for pollution from Sahara than for pollution from NA.

5. OPTICAL CHARACTERIZATION

Multiwavelength Raman lidar allows the characterization and identification of different aerosol types. The wavelength dependence of backscatter coefficient, extinction coefficient (Ångström exponent $å$), and lidar ratio (S_{355}/S_{532}) shows characteristic signatures (see Tab. 1). The results of Tab. 1 emphasize the need for Raman lidar observations at two extinction channels.

Clean marine aerosols are characterized by a neutral spectral slope of backscatter and extinction and by lidar ratios below 30 sr. Anthropogenic particles show Ångström exponents between 1 and 2, lidar ratios at 532 nm from 30 – 80 sr. The lidar ratios at 355 nm are larger than those at 532 nm. Ångström exponents and 532-nm lidar ratios of forest-fire smoke are similar to the values of anthropogenic pollution, but in this case S_{355}/S_{532} is smaller than 1. Mineral dust particles observed over Leipzig do not show a spectral dependence of the backscatter coefficients. But extinction at 355 nm is larger than at 532 nm because of light absorption in the UV wavelength range.

The contribution of the free-tropospheric aerosol to the total optical depth (τ_{FT}/τ) depends more on source regions than on aerosol types. The values of 20%–30% are similar for anthropogenic pollution and for forest fire smoke from NA while the contribution of lofted layers from India over the Indian Ocean or from the Sahara over Leipzig is about 50%.

6. MICROPHYSICAL PROPERTIES

Fig. 3 (top) shows effective radius versus Ångström exponent for all aerosol types. There is a rather clear separation between anthropogenic pollution from NA or Europe and forest-fire smoke. The largest particles on average are found for forest-fire smoke. The mean effective radius is 0.34±0.05 µm. Considerably smaller particles are found for anthropogenic pollution from

Tab. 1. Characteristic signatures of different aerosol types observed during INDOEX,[1] ACE 2,[2] and EARLINET (2000-2003)[3]

source	å	S_{532}	S_{355}/S_{532}	τ_{FT}/τ
clean marine PBL[1]	0.1	< 30 sr	≈ 1	—
North India[1]	1.2	50 – 80 sr	> 1	0.5
South India[1]	0.9	30 – 50 sr	> 1	0.5
SE Asia[1]	1.5	30 – 70 sr	> 1	0.3
anthr. pollution from Europe[2]	1.4	35 – 55 sr	> 1	0.6
European PBL[3]	1.4	40 – 60 sr	> 1	—
anthr. pollution from NA[3]	1.7	40 – 50 sr	> 1	0.2
anthr. pollution from north of 70° N[3]	2.1	50 – 90 sr	> 1	0.4
forest-fire smoke from NA and Siberia[3]	1	30 – 60 sr	< 1	0.3
Sahara[3]	0.7	50 – 75 sr	> 1	0.5

NA. The mean effective radius is 0.17±0.02 µm. Outflow of anthropogenic pollution from Europe shows a comparably low effective radius of 0.15±0.06 µm. Particles from South Asia are in between the other two particle types. The mean effective radius is 0.2±0.08 µm.

Fig. 3 (bottom) shows the ssa vs. the imaginary part of the complex refractive index. South Asian pollution covers a wide range of numbers from 0.8–1. The mean value is 0.91±0.06. Most of the values for ACE 2 are >0.9. The mean value is 0.95±0.06. A slightly lower mean ssa of 0.93±0.02 is found for anthropogenic pollution from NA. A similarly large mean value of 0.93±0.03 has been found for the free-tropospheric forest-fire smoke observed in 2003.
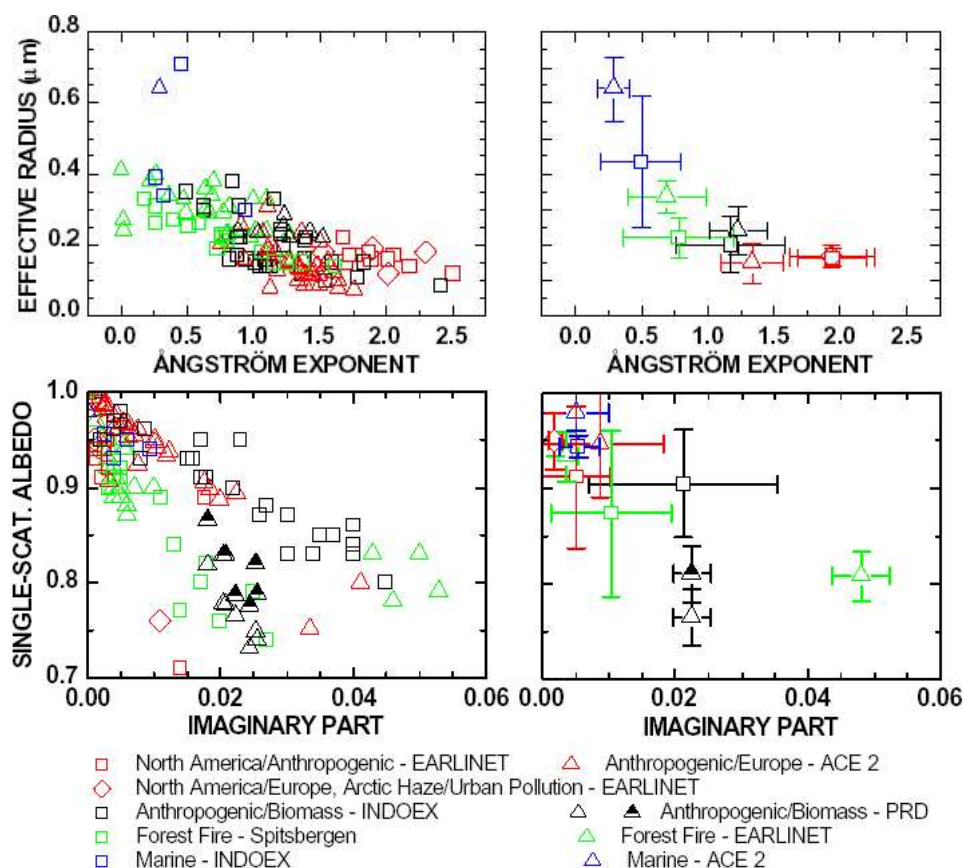
Fig.3. Effective radius vs. Ångström exponents (top) and ssa vs. imaginary part of the complex refractive index (bottom). Left panels show results for single measurements, right panels show the respective mean values of the different aerosol types. Results from Pearl River Delta near Hong Kong in south China (one of the major source regions of anthropogenic pollution in southeastern Asia)[12], and from Spitsbergen are presented in addition to the aerosol types discussed in the text.

7. REFERENCES

1. Mattis I. et al., Multiyear aerosol observations with dual-wavelength Raman lidar in the framework of EARLINET, *J. Geophys. Res.* 109, D13,203, doi:10.1029/2004JD004 (2002).

2. Althausen A. et al., Scanning 6-wavelength 11-channel aerosol lidar, *J. Atmos. Ocean. Tech.* 17, 1469-1482 (2000).

3. Müller D. et al., Retrieval of physical particle properties from lidar observations of extinction and backscatter at multiple wavelengths, *Appl. Opt.* 37, 2260-2263 (1998).

4. Kolgotin A. and Müller D., 2-Dimensional Regularization for the Retrieval of Profiles of Microphysical Aerosol Properties from Multiwavelength Raman Lidar, *this proceedings* (2006).

5. Bösenberg et al., EARLINET: A European Aerosol Research Lidar Network to Establish an Aerosol Climatology, Report No. 348, *Tech. rep.*, Hamburg, Germany (2003).

6. Ansmann A. et al., European pollution outbreaks during ACE 2: Optical particle properties inferred from multiwavelength lidar and star/Sun photometry, *J. Geophys. Res.* 107, 4259, doi: 10.1029/2001JD001 (2002).

7. Franke K. et al. Optical properties of the Indo-Asian haze layer over the tropical Indian Ocean, *J. Geophys. Res.* 108, 4059, doi: 10.1029/2002JD002 (2003).

8. http://www.arl.noaa.gov/ready/open/traj.html

9. Stohl, A. et al., Accuracy of trajectories as determined from the conservation of meteorological tracers. *Q. J. Roy. Met. Soc.* 124, 1465-1484 (1998).

10. Sheele, M. et al., Sensitivity of trajectories to data resolution and its dependence on the starting point: in or outside the tropopause fold. *Meteor. Appl.* 3, 267-273 (1996).

11. Stohl, A. et al., A density correction for Lagrangian particle dispersion models. *Bound. -Layer Met.* 90, 155-167 (1999).

12. Ansmann et al., High aerosol load over the Pearl River Delta, China, observed with Raman lidar and Sun photometer, *Geophys. Res. Lett*, 32, doi:10.1029/2005GL023094 (2005).